Acoustic interferometers based on two-dimensional arrays of rigid cylinders in air

Lorenzo Sanchis and Andreas Håkansson
Departamento de Física Teórica de la Materia Condensada, Facultad de Ciencias, Universidad Autónoma de Madrid, 28049 Madrid, Spain

Francisco Cervera
Departamento de Física Aplicada, ETSI Telecomunicación, Universidad Politécnica de Valencia, 46022 Valencia, Spain

José Sánchez-Dehesa*
Departamento de Física Teórica de la Materia Condensada, Facultad de Ciencias, Universidad Autónoma de Madrid, 28049 Madrid, Spain

(Received 11 August 2002; revised manuscript received 28 October 2002; published 30 January 2003)

This work presents a comprehensive study of acoustic interferometers based on sonic crystals, such as the one reported by Cervera *et al.* in Phys. Rev. Lett. **88**, 023902 (2002). This kind of interferometers consist of a slab of rigid cylinders in air put in a periodic configuration. Their performance as a function of thickness and symmetry configuration (square and hexagonal) is analyzed by our setup, which obtains the reflectance spectra using the standing wave ratio technique. Experimental observations are fairly well simulated by a self-consistent wave theory that incorporates all orders of multiple scattering. An homogenization procedure shows that sound propagation inside the hexagonal-based crystals is isotropic while it is biaxial inside the square-based crystals. A method able to extract the acoustic band structure from the reflectance spectra of the finite crystals under study is also described. Finally, the robustness of the interference effects is also studied as a function of positional disorder inside the unit cells in the lattice.

DOI: 10.1103/PhysRevB.67.035422 PACS number(s): 68.60.Bs, 43.20.+g, 43.58.+z, 68.60.−p

I. INTRODUCTION

A photonic crystal[1] is to light waves what a semiconductor is to electrons: it allows the passage of waves at some energies but no others. In other words, the allowable energies are distributed in bands. In a similar manner, a fluid medium with a periodic density variation define a system called a sonic crystal (SC), which forbids sound propagation at certain frequencies.[2] The fundamental reason for the phenomenon of band structure is the multiple scattering of waves in a periodic configuration of scatterers.

Recently, experimental observations have demonstrated that SC's consisting of periodic arrays of metallic cylinders (i.e., rigid scatterers) in air show stop-band and pass-band regions.[3–11] On one hand, the presence of stop bands have led to the proposal of using the SC's to construct a new generation of sound shields and filters.[3–10] On the other hand, their property of sound transmission in the pass-band frequencies has been recently used[11] to construct refractive devices such as an acoustic lens for focusing sound waves and also an acoustic interferometer that works similar to its lightwave counterpart. Experiments on more complex structures called phononic crystals, where the waves can have a mixed character (longitudinal and trasversal), have also been reported.[12–15] Most of the experiments report zero-order attenuation spectra of sound transmission across the periodic structure, just one work has reported reflectance properties.[9]

The theoretical description of sonic and phononic crystals has employed two main strategies. One consists on band structure calculations[3–7,10,16,17] of the corresponding infinite system in order to match the gaps in the dispersion relation with the attenuations in the transmission spectra. The other calculates the transmission spectra by different algorithms such as the transfer matrix method,[18] finite differences,[19–21] or by multiple scattering.[9,22,23] The drawback of the first approach is that additional attenuation bands can appear in the zero-order spectra due to two reasons: (1) the presence of deaf bands[4] in the dispersion relation and (2) the existence of diffraction effects above a certain cutoff frequency; i.e., the possible scattering of sound to Bragg orders larger than the especular when it leaves the SC.[5] On the other hand, the other approaches usually produce good experimental description, but sometimes interesting physical phenomena are shielded if not a further analysis of the spectra is completed by studying the symmetry character of the eigenmodes and their dispersion relation.

The purpose of this paper is to present a comprehensive analysis of structures similar to the one introduced in Ref. 11 used as an acoustic interferometer. Experiments have been performed for several structures with variable thickness in two different symmetry configurations: hexagonal and square. Theoretically, a self-consistent multiple scattering approach has been developed containing some improvements over the ones previously reported. Our simulations will be focused on the reflectance properties of these structures, which is a topic scarcely treated in the literature. It will be shown that reflectance spectra is a good spectroscopic tool characterizing the internal modes of SC clusters and can be used to obtain partially the two-dimensional (2D) acoustic band structure. Thus, modes having their wavefronts parallel to the surfaces of the cluster produce well defined zero reflectance features in the spectra when they are excited by sound waves impinging the cluster perpendicularly to its sur-

faces. These modes can be assigned to Bloch modes of the 2D band structure.

The frequency and symmetry of acoustical modes predicted by the multiple scattering approach characterize fairly well the resonance features observed in the spectra. Moreover, the spectra in the frequency regions below and above the gaps are similar to the ones expected from homogenized layers, whose characteristic impedance and effective sound velocity have been obtained by a fitting procedure.

As a result of our studies we concluded that the sound velocity inside SC's verify the following properties: (i) it is always lower than in air, (ii) it depends on the crystal thickness, and (iii) it also depends on the parameters characterizing the crystal (i.e., the lattice symmetry and the fraction of volume occupied by the cylinders). Particularly, it has been demonstrated that hexagonal lattice is isotropic with regards to sound propagation while the square lattice behaves biaxially. Moreover, the reflectance of the SCs' slabs is small and depends on the filling fraction; it increases as the filling fraction increases. Finally, the fairly good agreement found between theory and experiments has lead us to make predictions about the robustness of the interference effects as a function of the disorder in the lattice.

The paper is organized as follows. The theoretical approach is presented in Sec. II while the experimental setup together with the sample descriptions are given in Sec. III. The comparison between experiments and calculations are presented in Sec. IV, where it is explained how to get the band structure from the reflectance minima, and the results of the homogenization procedure are also discussed. In Sec. V the predictions about disordering effects are reported. Finally, Sec. VI summarizes the work.

II. THEORETICAL APPROACH: THE SELF-CONSISTENT WAVE THEORY

A simplified approach (only including double-scattering terms) of the treatment described below has been successfully applied to study the reflectance properties of a cluster of 35 cylinders.[9] A complete self-consistent procedure including all order of multiple scattering, which follows the seminal work of Twersky,[24] has been reported by Chen and Ye[23] to study the transmission spectra of large structures. The procedure is briefly described below. In particular, we introduce a symmetry of the matrix elements that reduces the computational effort of the numerical code.

Let us consider a cluster of N cylinders located at positions $\vec{R}_\beta$ ($\beta=1,2,\ldots N$) and radius ρ_β. $\vec{R}_\beta$ is a vector in the XY plane. The geometry of the problem and the variable definitions are shown in Fig. 1.

If a external wave P^{ext} with temporal dependence $e^{-i\omega t}$ impinges the cluster, the total field around the cylinder α is a superposition of the external field and the radiation scattered by the rest of cylinders β:

$$P_\alpha(x,y)=P^{\text{ext}}(x,y)+\sum_{\beta\neq\alpha}^{N} P_\beta^{\text{scatt}}(x,y), \tag{1}$$

where P_β^{scatt} is the field scattered by the β cylinder.

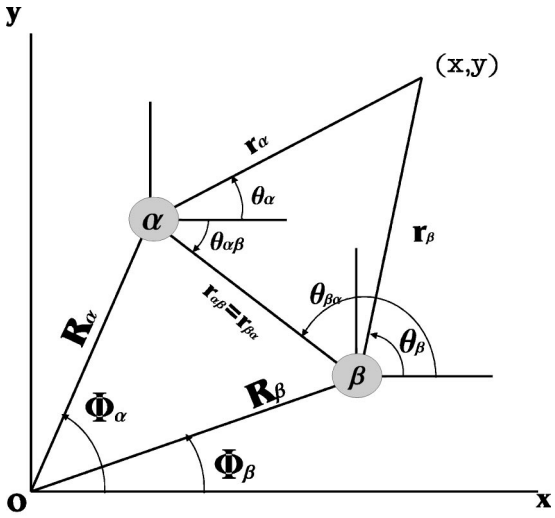

FIG. 1. Coordinate systems and definition of variables employed in the equations of the multiple-scattering algorithm (see Sec. II).

Those fields can be expanded as a combination of Bessel functions centered at the cylinder position. If the multipole coefficients are $(B_\alpha)_l$, $(S_\alpha)_l$, and $(A_\beta)_l$, for P_α, P_β^{ext}, and P^{scatt}, respectively, the expression above can be cast into the following relation between coefficients:

$$(B_\alpha)_l=(S_\alpha)_l+\sum_{\beta=1}^{N}\sum_{l'=-\infty}^{l'=\infty}(G_{\beta\alpha})_{ll'}(A_\beta)_{l'}, \tag{2}$$

$G_{\beta\alpha}$ being the propagator from β to α whose components are

$$(G_{\beta\alpha})_{ll'}=(1-\delta_{\alpha\beta})e^{i(l'-l)\theta_{\alpha\beta}}H_{l'-l}^{(1)}(\kappa r_{\alpha\beta}), \tag{3}$$

where $\delta_{\alpha\beta}$ is the Kronecker delta ($\delta_{\alpha\beta}=1$ if $\alpha=\beta$, and $\delta_{\alpha\beta}=0$ if $\alpha\neq\beta$).

Notice that coefficients S_α are known, but B_α and A_α are not. The boundary conditions at the cylinder's surfaces relates B_α and A_α. Though the experiments involved hollow aluminum (Al) cylinders, here, we use the simplifying assumption of rigid cylinders. This approach works fairly well in the theoretical description of experiments in the range of frequencies under study.[4,5] In addition, the thickness of the metallic tubes and the huge density contrast between Al and air justified the approach.[25] The t-scattering matrix relates A_2 and B_2

$$(t_\alpha)_{ll'}=\frac{J_{l-1}(\kappa\rho_\alpha)-J_{l+1}(\kappa\rho_\alpha)}{H_{l+1}^{(1)}(\kappa\rho_\alpha)-H_{l-1}^{(1)}(\kappa\rho_\alpha)}\delta_{ll'}. \tag{4}$$

Introducing these coefficient in Eq. (2) and after an easy algebra we arrive at

$$(A_\alpha)_l-\sum_{\beta=1}^{N}\sum_{l'=-\infty}^{l'=\infty}(t_\alpha G_{\beta\alpha})_{ll'}(A_\beta)_{l'}=(t_\alpha S_\alpha)_l. \tag{5}$$

By truncating the angular momentum within $|l'|\leqslant l_{\max}$, Eq. (5) reduces to a linear equation where the dimension of the relevant matrix is $N(2l_{\max}+1)\times N(2l_{\max}+1)$. Thus, in

matrix form $\mathcal{M}A=S$, where A and S are column matrices with elements $A_{1l}, A_{2l}, \ldots A_{Nl}$ and $t_{1l}S_{1l}, t_{2l}S_{2l}, \ldots t_{Nl}S_{Nl}$, respectively. $\mathcal{M}$ is a square matrix where each element is a matrix of dimension $(2l_{\max}+1)\times(2l_{\max}+1)$. In short, the matrix elements can be expressed by

$$(\mathcal{M}_{\alpha\beta})_{ll'}=\delta_{\alpha\beta}\delta_{ll'}-(t_\alpha G_{\alpha\beta})_{ll'}(1-\delta_{\alpha\beta}). \tag{6}$$

When the structure contains a huge amount of cylinders, the CPU time required in the calculations can be reduced to the half by using the following relation between the matrix elements:

$$(\mathcal{M}_{\alpha\beta})_{ll'}=\left[(1-\delta_{\alpha\beta})(-1)^{(l'-l)}\frac{(t_\beta)_{ll'}}{(t_a)_{ll'}}+\delta_{\alpha\beta}\right](\mathcal{M}_{\beta\alpha})_{ll'}. \tag{7}$$

This relation is obtained from the properties of the polar variables $\theta_{\beta\alpha}-\theta_{\alpha\beta}=\pi$, and $r_{\alpha\beta}=r_{\beta\alpha}$. These properties imply that $(G_{\alpha\beta})_{ll'}=(-1)^{(l'-l)}(G_{\beta\alpha})_{ll'}$, which introduced into Eq. (6) gives the identity in Eq. (7).

Finally, the unknown coefficient **A** can be easily obtained by matrix inversion, and the pressure field at any point outside the cylinders is given by

$$P(x,y)=P^{\text{ext}}(x,y)+\sum_{\alpha=1}^{N}P_\alpha^{\text{scatt}}(x,y)=P^{\text{ext}}(r,\theta)$$
$$+\sum_{\alpha=1}^{N}\sum_{l=-\infty}^{l=\infty}(A_\alpha)_l H_l^{(1)}(\kappa r_\alpha)e^{il\theta_\alpha}. \tag{8}$$

The normal modes of a finite system may be obtained by solving the following secular equation, which is obtained from Eq. (5) in absence of external incident wave; i.e., $(S_\alpha)_{l'}=0$:

$$D_N(\omega)=\det[\,\delta_{\alpha\beta}\delta_{ll'}-(t_\alpha G_{\alpha\beta})_{ll'}(1-\delta_{\alpha\beta})]=0. \tag{9}$$

The solutions are complex resonance frequencies $\omega=\omega'-i\omega''$. The real part ω' gives the eigenfrequency of the normal mode and its lifetime in this resonator can therefore be estimated by $\tau=1/(2\omega'')$. The procedure explained above is formally equivalent to the one previously employed to study clusters of 2D photonic crystals.[26,27]

The acoustic structure of an infinite periodic system can be obtained taking into account that Bloch theorem applies to the coefficients as

$$(A_\beta)_{l'}=e^{\vec{k}\cdot\vec{R}_\beta}(A_0)_{l'}, \tag{10}$$

where $\vec{k}$ is a wave vector contained in the first Brillouin zone of the Bravais lattice defined by the vectors $\vec{R}_\beta$. For the case of a single scatterer per unit cell, like in the hexagonal and square lattices, the secular equation for the acoustic band modes is

$$\det[\,\delta_{ll'}-[tG(\vec{k};\omega)]_{ll'}(1-\delta_{\vec{R}})]=0, \tag{11}$$

where $t\equiv t_\alpha$ is the expression in Eq. (4), and

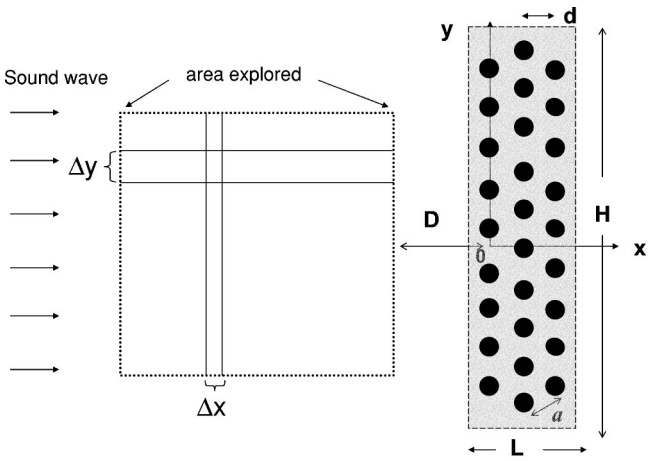

FIG. 2. Schematic view of the experimental set up employed in the experiments. The sample represents an hexagonal array with surfaces perpendicular to the ΓX direction of the lattice. It is made of 10×3 cylinders. The dotted rectangle in front of the sample defines the area explored by the robot. Measures are taken at points separated Δx along the X axis and Δy along the y axis. a is the lattice parameter $D\approx2a$, $d=a\sqrt{3}/2$. The shadowed region represents the effective dimension of the sonic crystal according to the criterium of Ref. 31; $L=3a\sqrt{3}/2$, $H=10a$.

$$[G(\vec{k};\omega)]_{ll'}=\sum_{\vec{R}}[G(\vec{R};\omega)]_{ll'}\exp(i\vec{k}\cdot\vec{R}), \tag{12}$$

where the sum $\Sigma_{\vec{R}}$ is over all lattice sites, and

$$[G(\vec{R};\omega)]_{ll'}\equiv(G_{0\beta})_{ll'}=(1-\delta_{\vec{R}})e^{i(l'-l)\theta_R}H_{l'-l}^{(1)}(\kappa R), \tag{13}$$

being $\vec{R}=\vec{R}_\beta-\vec{R}_0$, and κ is related to ω through the sound velocity in air. The expansion coefficients are calculated following the Ewald procedure.[28]

III. EXPERIMENTS

The experiments have been performed in a echo-free chamber. As a sound source we employed a collimated beam, which were obtained by placing an omnidirectional speaker at the focus of a parabolic reflector.

The SC samples are constructed by hanging cylindrical rods (1 m long) on a frame with the appropriate symmetry. In particular, arrays of hollow aluminum cylinders of external radius $\rho=2$ cm and thickness 2 mm were put in two different configurations; hexagonal and square. All the rows in a sample have the same length H, which in our samples is determined by 12 rods. A schematic view of the experimental setup is shown in Fig. 2. The parameter a in the hexagonal lattice is 6.35 cm, while in the square lattice is 11 cm. In other words, the fraction of volume f occupied by the rods in the hexagonal case is $f_h=(2\pi/\sqrt{3})(\rho/a)^2=0.360$ while for the square lattice $f_s=\pi(\rho/a)^2=0.104$. For the hexagonal lattice results are reported for three samples with three, four, and five layers of cylinders, which were constructed having their surfaces perpendicularly to the ΓX direction (distance between layers $d=a\sqrt{3}/2$). For the square lattice, the results

obtained in two samples with the same thickness (5 layers) are reported; one oriented along the ΓX direction ($d=a$), the other along the ΓM direction ($d=a/\sqrt{2}$).

In order to study the reflectance, pressure maps have been obtained in front of the sample by means of a computer-controlled automatic positioning system capable of sweeping a microphone through a grid of measuring points. Two steeper motors with a maximum resolution of 0.25 mm per step allows the movement along each X and Y axis. The pressure maps are obtained from a grid of 400 points; 50 points spaced $\Delta x=10$ mm along the X axis and 8 points spaced $\Delta y=40$ mm along the Y axis. The total area scanned by the map is 49 cm$\times$28 cm (see Fig. 2). Nevertheless, larger areas could be explored, if needed, by hand relocation of the whole frame of the robot.

Sound pressure measurements are automatically taken by means of a B&K 2144 frequency analyzer controlled by a GPIB interface. At each grid point the microphone samples the sound with a sampling frequency of 15 kHz. The pressure spectrum with a resolution of 8 Hz is obtained by the analyzer, which makes the FFT of the data recorded by the microphone. A total of 256 spectra have been taken to generate the averaged spectrum finally assigned to each grid point (x_i,y_i). Thus, for a given frequency, the root-mean-square (r.m.s.) pressure $P_{rms}(x_i,y_i)$ is obtained. To express the pressure in decibels we employ a reference pressure of 20 μPa, thus

$$L(x_i,y_i)(dB)=20\log_{10}[P_{\text{r.m.s.}}(x_i,y_i)/\text{Pref}]. \qquad (14)$$

The total time elapsed to construct one pressure map as described above is about 5 h.

IV. RESULTS AND DISCUSSIONS

A. Ordered structures

The acoustic band structures for the corresponding infinite systems are plotted in Fig. 3. They are obtained from the secular equation, Eq. (11). The gaps that forbids sound propagation fairly agrees with zero-order transmission experiments reported in Refs. 4–6. The hexagonal lattice has a complete acoustic gap at the region 2498–3104 Hz, which is determined by the gap in the ΓJ direction. Along the ΓX direction a pseudogap exists in the 2109–3474 Hz frequency region. On the other hand, the square lattice only shows a pseudogap along the ΓX direction: in the range 1308–1680 Hz.

A parameter of interest regarding the sound propagation in these structures is the sound velocity at large wavelengths, where the frequency increases linearly with the wave vector. In other words, at frequencies where the phase velocity ($c'=\omega/k$) and group velocity ($v_g=\partial\omega/\partial k$) coincide. Table I gives the numerical predictions, which shows that the sound propagates inside the SC at velocities lower than in air; their values depend on the filling fraction, being lower at higher f. The results for the hexagonal samples were reported before[11] and the velocity reduction, which was also demonstrated experimentally, were explained as a impedance effect that results in an effective increase of the air density.[29] From Table I we conclude that the hexagonal lattice behaves isotropically regarding sound propagation while the square lattices does biaxially. In this section it will be shown that these predictions made for periodic systems are supported by reflectance measurements as well as by numerical calculations based on the multiple-scattering technique, both performed in finite sytems.

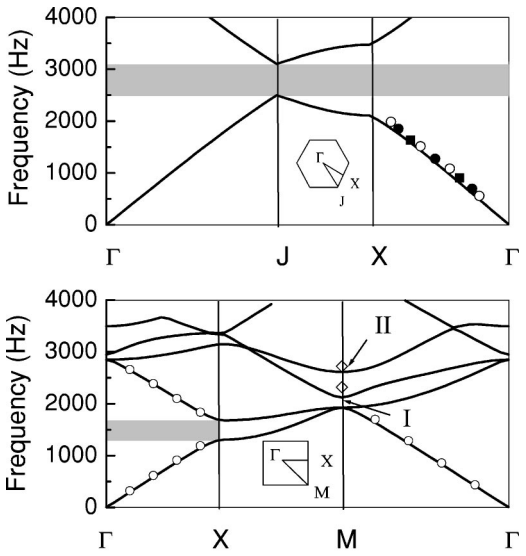

FIG. 3. (a) Acoustic bands of an hexagonal lattice (lattice parameter $a=6.35$ cm) of rigid cylinders (radius 2 cm) in air. (b) Acoustic bands for a square lattice ($a=11$ cm) of cylinders with equal radius. The insets show the corresponding Brillouin zones and the special points. The symbols represent the reflectance minima found in the spectra for the samples analyzed: three layers (full squares), four layers (full circles), and five layers (empty circles). The diamonds corresponds to minima whose associated mode are above the difraction limit (see text).

The pressure maps have been calculated by the multiple scattering approach described in Sec. II. The sums to the orders l of the Hankel functions in Eq. (8) have been truncated; only seven terms ($-3\leqslant l\leqslant 3$) were needed to get converged results (1% error). To compare with experiments, it has been defined a theoretical r.m.s. pressure $P^2_{\text{theo}}(x,y)=\frac{1}{2}|P(x,y)|^2$, which is the time-averaged square pressure at each point. The corresponding pressure (in dB) is

$$L_{\text{theo}}(x,y)(dB)=20\times\log_{10}(|P(x,y)|/\alpha), \qquad (15)$$

TABLE I. Sound speed (in m s^{-1}) inside a lattice of rigid cylinders in air. Its dependence on the filling fraction f along the two high symmetry direction in the two lattices hexagonal (h) and square (s) is given. The values are obtained from the slope of the first acoustic band near the zone center of the Brillouin zone.

Hexagonal lattice			Square lattice		
f_h	ΓX	ΓJ	f_s	ΓX	ΓM
0.051	329	329	0.058	329	331
0.090	320	319	0.104	318	317
0.202	298	298	0.234	293	302
0.360	276	277	0.415	266	277

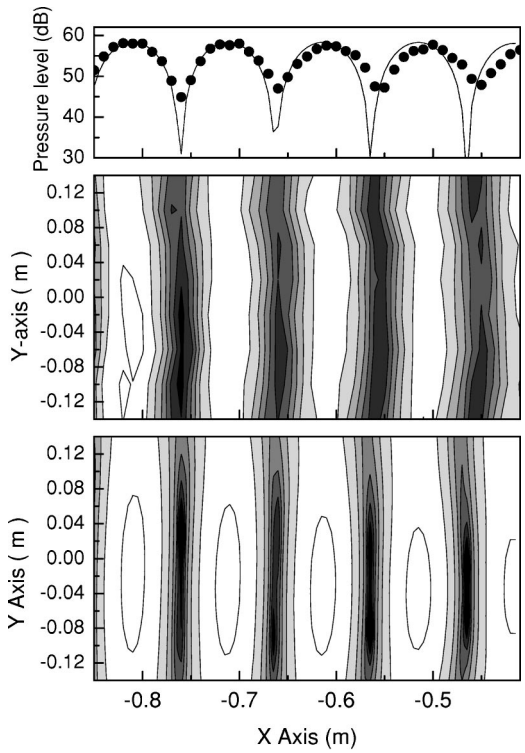

FIG. 4. (Top panel) root-mean-square (r.m.s.) pressure (in dB) measured (dots) and calculated (continuous line) along the x axis ($y=-0.05$ cm) in front of the sample made of five rows of cylinders put in a hexagonal configuration, the rows being perpendicular to the ΓX direction of the Brillouin zone. (Middle panel) Surface plot of the pressure $L(x,y)$ [Eq. (14)] obtained by the robot (lower panel). Surface plot of the pressure L_{theo} calculated by using the multiple scattering theory. The grey scale goes from black (low pressure) to white (high pressure).

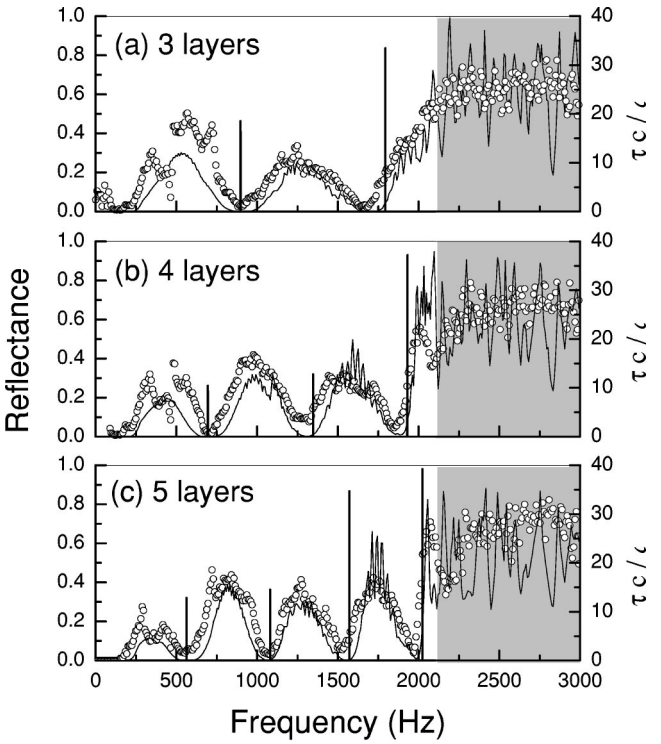

FIG. 5. Frequency dependence of the reflectance $\mathcal{R}$ measured (symbols) for samples based on a hexagonal array (lattice parameter $a=6.35$ cm) of rigid cylinders (radius 2 cm) in air. The continous lines represent the predictions obtained from the self-consistent wave theory introduced in Sec. II. The vertical bars represents the acoustical modes. The bar position gives the real part of the mode's frequency and its lifetime τ (in reduced units) is represented by the bar's height. The shadowed regions represent the band gap in the band structure of the corresponding infinite periodic systems (see Fig. 3).

where α is a parameter, which is adjusted to take into account that the actual incident pressure is not unity.

As a typical example, the top panel in Fig. 4 compares the pressure level measured and calculated along the x axis at $y=0$ for the case of a SC slab (five layers thick) with its surfaces perpendicular to the ΓX direction in the hexagonal configuration. It corresponds to the case of an incident wave of 1750 Hz, and the theoretical curve (continuous line) were obtained by using $\alpha=0.0025$ in Eq. (15). The center and bottom panels in Fig. 4 show the complete pressure maps measured and calculated, respectivelly. The agreement found between both maps demonstrates that the multiple scattering is a good approach to describe the observations.

The pressure maps in Fig. 4 show that a standing wave is formed in front of the sample that can be understood as due to the reflection suffered by the incident wave at the air/SC interfaces. This is a general result at any frequency. Below, we describe how the reflectance $\mathcal{R}$ is obtained from the standing wave.

At a given frequency ω, the standing wave for the case of a sample with $H\rightarrow\infty$ can be reduced to the general one-dimensional form

$$P(x)=Ae^{i(kx-\omega t)}+Be^{-i(kx-\omega t)}. \tag{16}$$

The standing wave ratio (SWR), which is defined as the ratio between the maximum pressure to the minimum pressure, can be put as a function of the reflection coefficient $\mathsf{r}=(B/A)=\sqrt{\mathcal{R}}$:

$$\text{SWR}=\frac{P_{\max}}{P_{\min}}=\frac{A+B}{A-B}=\frac{1+r}{1-r}. \tag{17}$$

From here, $\mathcal{R}$ can be cast as a function of SWR:

$$\mathcal{R}=|r|^2=\frac{\text{SWR}-1}{\text{SWR}+1}. \tag{18}$$

Though our samples are finite in the direction perpendicular to the impinging wave (the y axis in Fig. 2), the pressure pattern along the x axis effectively behaves as an ideal standing wave (see Fig. 4) and, therefore, the expression for $\mathcal{R}$ above has been applied.

A word of caution has to be given, Eqs. (17), (18) used SWR in decimal units, which can be extracted from the pressure maps (in dB) by using $\text{SWR}=10^{\text{SWR}(dB)/20}$. Thus, from experiments, $\text{SWR}_{\text{exp}}(dB)=L_{P\,\max}(dB)-L_{P\,\min}(dB)=20\times\log_{10}[(1+r)/(1-r)]$, while from the calculated maps, $\text{SWR}_{\text{theo}}(dB)=20\times\log_{10}(|P_{\max}|/|P_{\min}|)$.

Figures 5 and 6 plot the reflectance $\mathcal{R}$ in SC slabs based

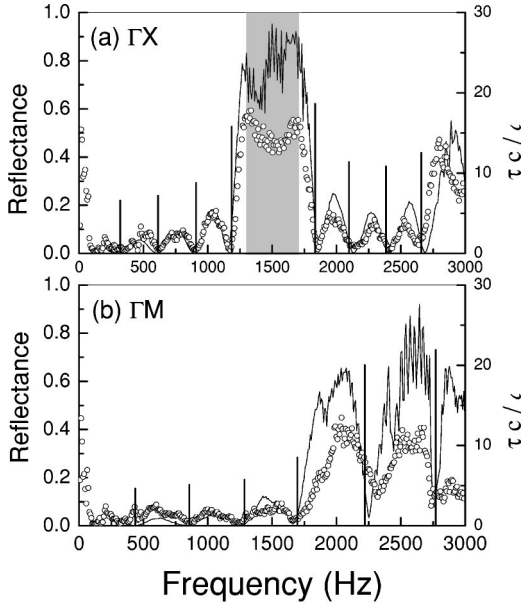

FIG. 6. Frequency dependence of the reflectance $\mathcal{R}$ measured (symbols) in samples based on a square array (lattice parameter $a=11$ cm) of rigid cylinders (radius 2 cm) in air. Results for samples of dimension 12×5 cylinders oriented along the two high symmetry directions in the lattice are shown. The continous lines represent the result obtained by the self-consistent wave theory introduced in Sec. II. The vertical bars represents the acoustical modes. The bar position gives the real part of the mode's frequency and its lifetime τ (in reduced units) is represented by the bar's height. The shadow region represent the band gap in the band structure of the corresponding periodic system (see Fig. 3).

on hexagonal and square symmetry, respectively. Figure 5 also presents the reflectance dependency of the slab thickness, while Fig. 6 shows the behavior along the two high symmetry directions in the square lattice. Both figures show that experimental observations (symbols) are fairly described by the multiple-scattering theory (continuous lines), where a plane wave with a κ-wave vector perpendicular to the air/SC interface is employed as the incident sound. Experiment and theory demonstrate that $\mathcal{R}$ oscillates similar to the reflectivity of a Fabry-Perot cavity for light waves. The experimental spectra also show additional features (peaks and shoulders) in between the zero reflectance frequencies. Those features clearly appear in the hexagonal samples (see the low frequency regions in Fig. 5) and their position and shape are maintained in the three samples anlyzed. Their observation in the spectra from the square based samples (see Fig. 6) is more dificult due to their low reflectance. The origin of these features can be atributed to internal modes (of symmetry different to the ones responsible of the zero reflectance features) that are excited by the fact that the actual impinging wave has not a plane wave front. They are of no interest in the present work and will be analyzed elsewhere.

The vertical lines in Figs. 5 and 6 indicate the location of the acoustical modes (resonances) responsible of the zero reflectance features in the spectra. They are computed as the roots of $\det(\mathcal{M})=0$ [see Eq. (9)] and their symmetry match the ones of the modes responsible for the similar phenomenon in homogeneous slabs. As an example, Fig. 7 shows several modes associated to the square-based slab. These results about resonances will be discussed below in a separate subsection.

1. Homogenization

Now, it seems worthwhile to find an equivalence between the SC slab and a slab of some effective thickness L containing a homogenous fluid in which the sound travels with a velocity c_{eff}. The fact that $\mathcal{R}=0$ at frequencies ν_n (n integer) indicates that resonances exist inside the SC slab whose wavelength λ is such that the slab thickness L is an integer number of half wavelengths $L=n\lambda/2$; in other words, $\nu_n=n\,c_{\text{eff}}/(2L)$. With this simplified assumption the oscillating period is

$$\Delta\nu=\nu_{n+1}-\nu_n=c_{\text{eff}}/(2L). \tag{19}$$

Now, we assume that the front and rear surfaces of the crystal are perpendicular to the propagation direction and that the distance between each surface and the center of the first cylinder is half a layer separation. Take, for example, the [1,0] orientation of the square lattice slab, which corresponds to the sound transmission in the $\Gamma\rightarrow X$ direction; the crystal surfaces are put at $x=-a/2$, and $x=(M-1)a+a/2$, where it has been considered that the first and last row of cylinders are located at $x=0$ and $x=(M-1)a$, respectively (M is the number of layers). Such surface condition in which the following calculations are based is how the surface is normally defined in a solid.[30] The slabs' thicknesses are determined according to this surface definition. Thus, for the previously described slab $L=Ma$.

Therefore, by analyzing the period of the oscillations in $\mathcal{R}$, it is possible to obtain a first approach to the sound velocity inside an homogenized slab. However, the simple model under Eq. (19) does not make it possible to get the reflectance at the air/SC interface, which is the other parameter needed to characterize the SC. To accomplish this goal we fit $\mathcal{R}$ in the range of frequencies where the oscillations are observed with its analytical expression for a homogenized layer of thickness L[30]

$$\mathcal{R}=\frac{4\mathcal{R}_0\sin^2(\omega L/c_{\text{eff}})}{1+\mathcal{R}_0^2-2\mathcal{R}_0\cos(2\omega L/c_{\text{eff}})}, \tag{20}$$

where $\mathcal{R}_0=(Z_{\text{SC}}-Z_{\text{air}})^2/(Z_{\text{SC}}+Z_{\text{air}})^2$ is the reflectance at normal incidence at the single interface. The fits to results in Figs. 5 and 6 have been performed in a frequency region below the theoretically predicted bandgap onset. Thus, for the samples based on the hexagonal (square) symmetry the fitting is performed in the region 560–1910 Hz (510–1180 Hz). The fitted parameters are given in Table II (hexagonal samples) and Table III (square samples). Let us stress that because of Eq. (20) it is only possible to determine the ratio L/c_{eff}, and therefore, the value assigned to c_{eff} has been obtained from a value L previously fixed by the surface definition explained above. In spite of this uncertainity, the values c_{eff} compare firly well with the ones predicted for infinite systems (see Table I), which indicates that a few monolayers

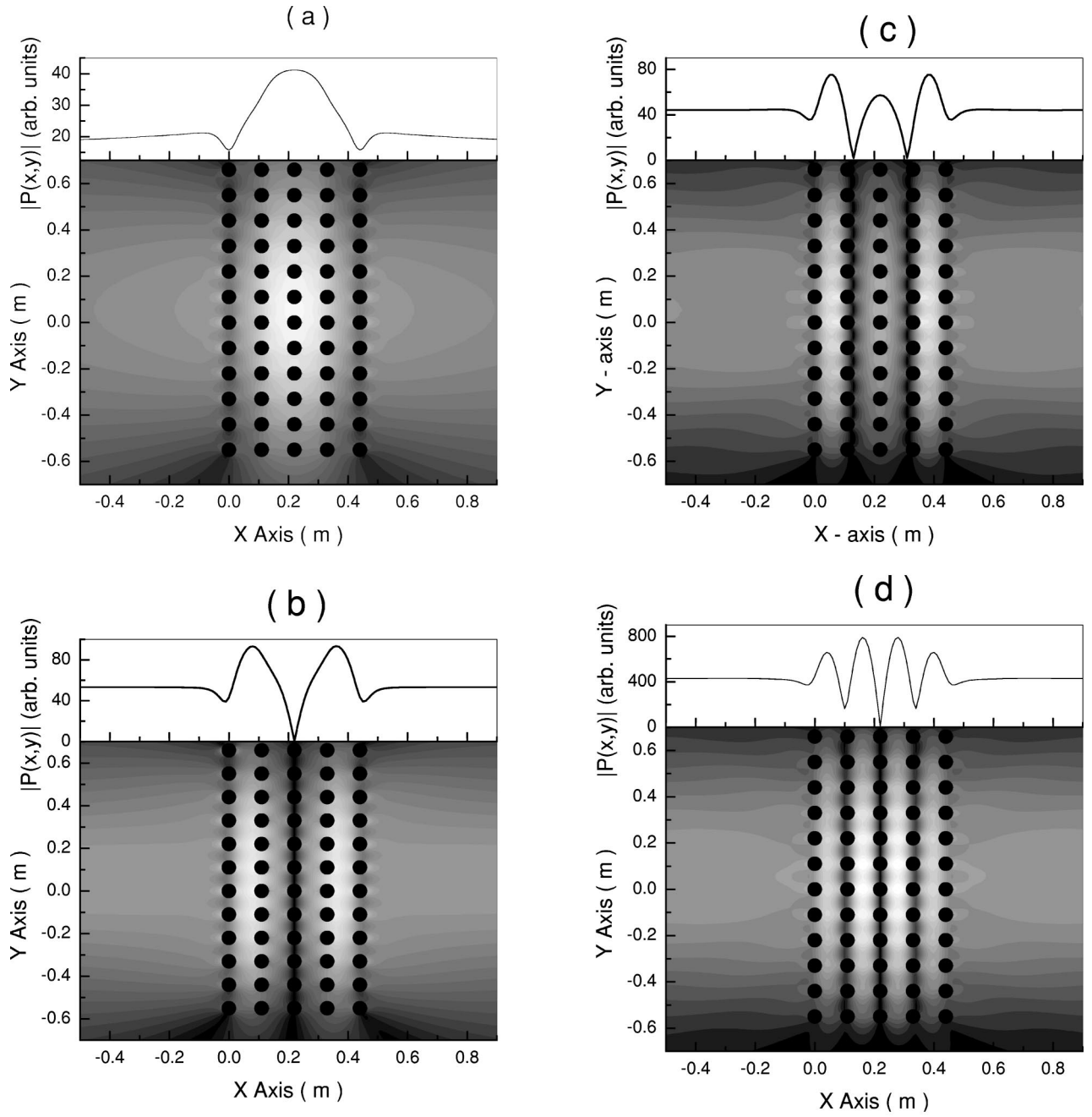

FIG. 7. Pressure map of the resonant modes responsible of the first four reflectance minima observed in the spectrum of Fig. 6(a). The modes have their maxima and minima along the ΓX direction. The line plots above give a section taken at $y=-0.05$ cm. Their calculated frequencies are (a) $\omega_1=318.8+324.5i$, (b) $\omega_2=613.8+215.05i$, (c) $\omega_3=909.3+176.0i$, and (d)$\omega_4=1186.2+97.9i$.

are enough to get bulk properties. With regards to $\mathcal{R}_0$, its values are very low for all the systems analyzed. The fact that it is larger in the hexagonal-based samples ($\mathcal{R}_0=0.11$–0.12) than in the square-based samples ($\mathcal{R}_0=0.017$–0.034) can be attributed to the larger filling fractions of the hexagonal structures.

In order to compare with the equivalent optical systems, it is convenient to know the ratio Z_{SC}/Z_{air}. From $\mathcal{R}_0$ this ratio is 1.25–1.27 for the hexagonal systems and 1.07–1.09 for the square ones, which have the same order of magnitude than the refraction index of optical materials typically employed in fabricating optical devices. Therefore, it can be stated that SC's can be used to fabricate acoustical refractive devices in a manner similar to the optical devices because they have the two following properties: (i) they are almost transparent to sound and (ii) they propagate the sound at lower velocity than in air.

2. Resonances of a finite SC slab

The photonic scattering by a finite size photonic crystal has been treated analogously to the electronic scattering by an atom in Ref. 26. In a similar manner, a finite cluster of

TABLE II. Parameters of a homogenized layer with thicknes L, whose reflectance $\mathcal{R}$ [Eq. (20)] fits the one of a sonic crystal slab made of a few layers of rigid cylinders (of radius 2 cm) put in a hexagonal configuration (lattice constant 6.35 cm) array of rigid cylinders. Slabs with different thickness, but all oriented along the ΓX direction in the lattice are considered (see Fig. 9). The values under the column experiment (theory) gives the fitted parameters to the experimental (theoretical) reflectance spectra.

Slab thickness	Three layers		Four layers		Five layers	
L (m)	0.165		0.22		0.275	
	theory	experiment	theory	experiment	theory	experiment
$\mathcal{R}_0$	0.11	0.11	0.11	0.11	0.12	0.12
$c_{eff}(m\,s^{-1})$	274	276	281	279	278	281

scatterers in air also contains resonances (acoustical modes) that are loosely confined in the cluster because of the SC impedance Z_{SC} being similar to that that of the surrounding media (the air). Therefore, an acoustical mode has a large field within the SC, which also does not vanish even outside the SC because the surroundings media do not forbids the presence of sound at the same frequency. Any of those modes may be regarded as an acoustical quasibound state and its energy spectra will have a finite width. Therefore, the scattering of a sound wave by this class of SC can create spectral features that will correspond to the acoustical modes whose eigenfrequency and lifetime can be accurately determined by the procedure described in Sec. II.

Figure 7 shows the pattern $|P(x,y)|$ of four acoustical modes associated to a cluster of 5×12 cylinders (black circles) put in a square configuration. They correspond to resonances producing zero reflectance features in the spectra shown in Fig. 4(a). The lineplots above each surface plot represent the pressure along the x axis at a fixed y coordinate ($y=-0.055$ m). The plots clearly show that these resonances have wave fronts parallel to the cluster surfaces, and their wavelenghts are such that the slab thickness is an integer number n of half wavelengths (a) $n=1$, (b) $n=2$, (c) $n=3$, and (d) $n=4$. Therefore, any of these modes will be excited by an external plane wave having the same frequency and impinging the cluster with a κ wave vector also perpendicular to the surfaces. This resonance excitation will produce a large transmission and it explains why the reflectance becomes zero. The frequencies (the real part) of all the resonances having the same symmetry along the ΓX direction (including the orders $n=5$, 6, 7, and 8) are defined by the position of the vertical lines in Fig. 6(a). On the other hand, the height of the vertical lines indicates the resonance lifetime τ_n, which is related the imaginary part of its frequency. Here τ_n is normalized in the unit of a/c (see the scale to the right). The agreement between resonance frequencies (the real part) and the existence of zero reflectance is almost exact and confirm the analogy with the behavior in an homogeneous slab.

A complete analysis of the acoustical modes responsible of the minima in the reflectance spectra have also been performed for the rest of samples under study. Their frequencies are represented by the vertical lines in Figs. 5 and 6 and they match fairly well with the reflectance minima. In regard with their symmetries, they are similar to the ones existing in homogeneous slabs, as it was shown in the examples of Figs. 7(a)–7(d). Nevertheless, the modes responsible for the fifth and the sixth minima for sound propagation along the ΓM direction in the square-based sample [see Fig. 6(b)] have a completely different symmetries. Their pressure patterns are given in Fig. 8. The left panel plots the mode responsible of the fifth minimum, which consists of a periodic distribution of 2D s type interacting orbitals almost confined in the space between cylinders. The right panel is the mode associated to the sixth minimum, which consists of 2D $d_{x^2-y^2}$-type interacting orbitals located in the same space. These symmetries

TABLE III. Parameters of the homogenized slab (thickness L) whose reflectance fits the one of a sonic crystal slab made with five rows of rigid cylinders (radius 2 cm) put in a square confuration (lattice constant 11 cm). Two different slabs were studied, each one oriented along one of the two high symmetry directions in the lattice. The values under the column experiment (theory) gives the fitted parameters to the experimental (theoretical) reflectance spectra.

	ΓX		ΓM	
L (m)	0.55		0.47	
	Theory	Experiment	Theory	Experiment
$\mathcal{R}_0$	0.034	0.034	0.017	0.019
$c_{eff}(m\,s^{-1})$	327	332	327	330

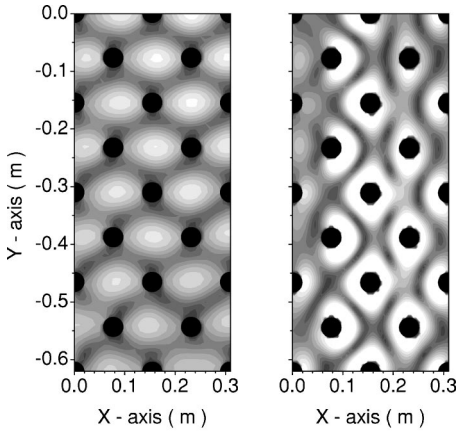

FIG. 8. Pressure map of the two acoustical modes responsible for the fifth (left panel) and sixth (right panel) reflectance minima of spectra shown in Fig. 6(b). Only the pressure in the lower half of the cluster is represented.

are originated by the fact that the modes' frequencies are above the diffraction limit (i.e., $\omega \geqslant 0.5 \times 2\pi c/a_s$, where a_s is the surface parallel period, $a_s = \sqrt{2}a$).

The correspondence found between resonance modes and reflectance minima can be used to obtain the acoustic band structure below the diffraction limit in a manner similar to the one developed in photonic crystal slabs.[32] In other words, it is expected that the large transmission is associated to Bloch states of the crystal. Equation (20) shows that the minima of $\mathcal{R}(\omega)$ are at the crystal momentum $k_n = (n/M) \times (G_1/2)$, G_1 is the first reciprocal lattice vector along the propagation direction, M is the number of layers and n being an integer ($n = 1,2, \ldots$). Following this procedure, the band dispersion determined from the reflectance minima obtained with the hexagonal-based samples [$G_1 = 4\pi/(a\sqrt{3})$] having $M = 3$, 4, and 5 layers (see Fig. 5) are represented by symbols in Fig. 3.

In regard to the spectra of the ΓX-square-based sample [Fig. 6(a)], where $G_1 = 2\pi/a$, a similar expression for the crystal momenta can be employed for frequencies in the first band. Above the band gap, it is convenient to express k within the reduced-zone scheme.[33] Thus, the frequencies at which the reflectance minima are located can be associated with $k_m = (G_1/2)(1 - m/M)$, where $1 \leqslant m \leqslant M$, $m = 1$ should be associated with the first peak above the pseudogap, $m = 2$ with the second peak, etc.; the white circles in Fig. 2 represent the results.

For the ΓM-square-based sample [Fig. 3(b)] the procedure described is not valid for the fifth and sixth minima because they are above the diffraction limit. Nevertheless, their high symmetry indicate that they must be associated to states at the Γ point of the BZ. Therefore, we analyzed the pressure pattern of every state of the periodic structure looking for the ones with very same symmetries. Figures 9(a) and 9(b) show the pressure pattern of those states, which belongs, respectively, to the third and fourth bands in the dispersion relation. The diamonds in Fig. 3 represents the reflectance minima ($\nu_5 = 2320$ Hz and $\nu_6 = 2726$ Hz) of these two modes. The discrepancy of about 100 Hz between reflectance minima and mode frequencies ($\nu_I = 2123$ Hz; $\nu_{II} = 2614$ Hz) in the acoustic band structure (see Fig. 3) can be attributed to finite size effects. In fact, a better agreement is obtained if the comparison is made with the resonances calculated by the scattering method for the exact cluster ($\nu_5 = 2219$ Hz and $\nu_6 = 2770$ Hz).

To conclude, the procedure described above supports the reflectance measurements as a useful tool able to get the band structure of SC by following a procedure applied in photonic crystal.[33] To the best of our knowledge, this is the first work where this procedure has been employed in SC.

It is also interesting to notice how the lifetime of the resonances increase when their frequencies are closer to the acoustic band edges. This behavior is a consequence of the underlying band structure: when the wavevector associated to the resonance is closer to the acoustic band edges, its group velocity is lower and, therefore, has a larger lifetime. A similar behavior was also reported for photonic modes in 2D photonic clusters.[26]

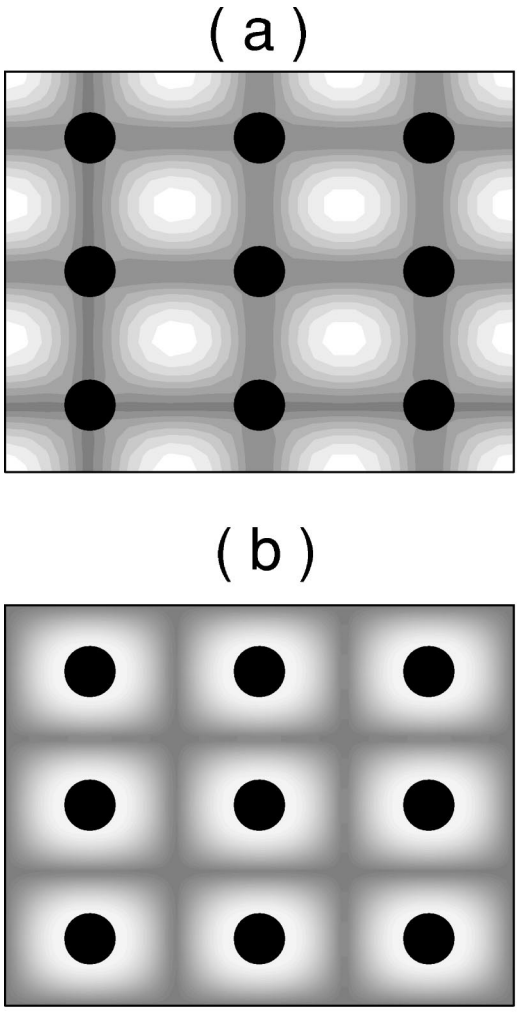

FIG. 9. (a) Pressure patern of the third state at the Γ point of the Brillouin zone in a square lattice of rigid cylinders in air (I in Fig. 3). (b) Pressure pattern of the fourth state (II in Fig. 3). The dots represents the positions of the cylinders in the lattice.

B. Disordered structures

The results presented above support the theoretical model employed in the description of the acoustic interferometers. In particular, the agreement with the experimental spectra indicates that a sound wave with a plane wave front is a good approach to the actual sound waves generated in the experiments. These facts allow us to go a step further and, therefore, this section is devoted to present the predictions obtained with our self-consistent wave theory regarding the robustness of the interference phenomenon against disorder in the lattice.

Here, only one class of disorder will be considered, which we named ''weak disorder'' because the periodicity of the lattice (hexagonal or square) is maintained but the cylinder's position in each unit cell is chosen at random. Thus, it will be assumed that the cylinders' volume always is enclosed in the volume of the unit cell. Thus, for example, the cylinders' position inside a cell in the square lattice configuration is

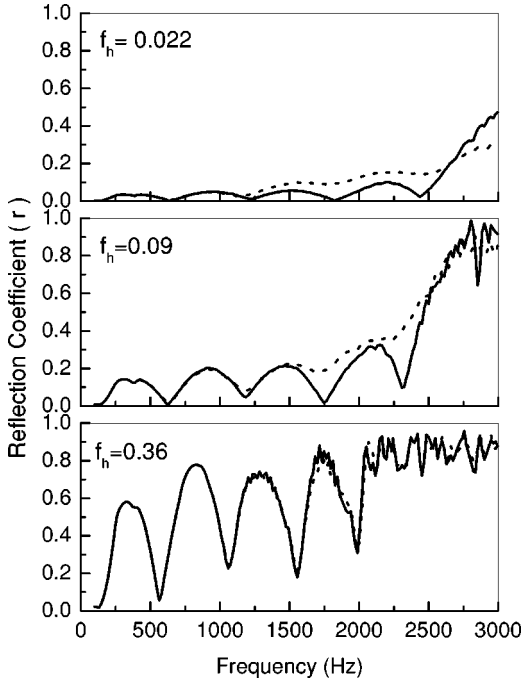

FIG. 10. Reflection coefficients r calculated with the multiple scattering algorithm for three different sonic crystal slabs (12×5 cylinders) with hexagonal symmetry ($a=6.35$ in Fig. 4). All the crystals are aligned along the ΓX direction but the cylinder's radius is different in each case (the filling fractions f_h are given). The continouos lines represent results for the perfectly ordered lattice. The dotted lines give the average of the results obtained from five ''weak disordered'' distributions of cylinders (see text).

$$x=\varepsilon\times(a/2-R),$$

$$y=\varepsilon'\times(a/2-R), \tag{21}$$

where ε and ε' are random numbers that take values in the segment [-1,1]; the value $\varepsilon=\varepsilon'=0$ gives the position in the ordered lattice. A similar condition is used to determine the positions inside the cells of the hexagonal lattice.

In order to compare with ordered structures, the coefficient r assigned to a disordered lattice is an average of the coefficients calculated in five different configurations. Thus, Fig. 10 shows the frequency dependence of r obtained for a cluster made with five layers of cylinders (each layer has 12 cylinders) with hexagonal symmetry, the layers are aligned perpendicularly to the ΓX direction. The dependence with the filling fraction f_h is also shown. The continuous lines give the results obtained for the ordered cluster while the dotted lines represent the ones obtained when the positions of the cylinders are random inside each unit cell in the lattice. Notice that conservation of the Bravais lattice does not guarantee the conservation of oscillations in r at frequencies outside the bandgap because the Bloch theorem cannot be applied in the disordered structures; there is not a mode in the SC with a defined $\vec{k}$ vector to allow the sound propagation inside the cluster. Therefore, the agreement between theory and experiment is not possible at any frequency because of the nonexistence of an underlying dispersion relation. Instead, the agreement is only possible at frequency regions where the standard homogenization procedure works well. Thus, notice that at $f_h=0.022$, the agreement is found for impinging wavelenghths above a cutoff wavelength λ_c larger than the slab thickness ($L=27.5$ cm); $\lambda_c=30$ cm. For $f_h=0.09$ the cutoff is $\lambda_c=23$ cm, which also correspond to the total accessible length of the cylinders along the sound incident direction. Finally, for a large filling fraction $f_h=0.36$ the cylinders positions have a volume accessible that is only a 8% of the cell's volume; the cylinders positions in the disordered cluster are only perturbed with respect to the ideal positions and, therefore, the agreement with the results in the ordered structure covers a large frequency region. In conclusion, the hexagonal clusters with ''weak disorder'' have a reflectance coefficients r that mimic fairly well the behavior of perfectly ordered clusters, being the agreement worse for decreasing filling fractions.

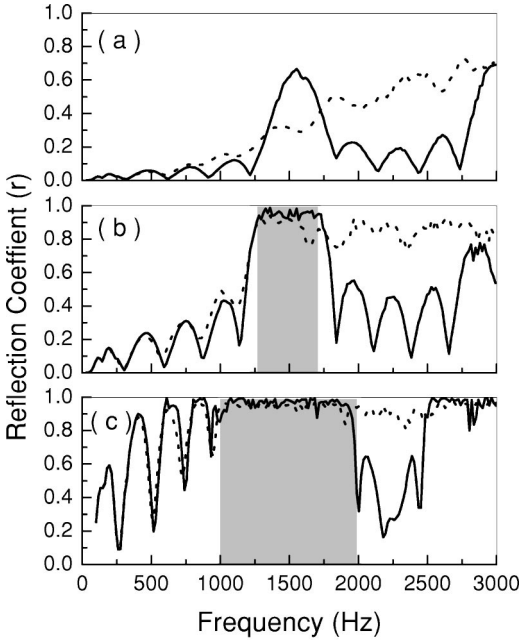

FIG. 11. Reflection coefficient of a sample (12×5 cylinders) with square symmetry ($a=11$ cm) oriented along the ΓX direction. Three different filling fractions f_s are studied: (a) $f_s=0.022$, (b) $f_s=0.103$, and (c) $f_s=0.230$. The continouos lines represents results for the perfectly ordered lattice. The dotted lines give the average of the results obtained with five ''weak disordered'' distributions of cylinders (see text). The shadowed regions represent the bandgaps in the band structure of the corresponding periodic systems.

Figure 11 shows r corresponding to SC clusters made of five rows of cylinders (each row having 12 cylinders) based on an square distribution of cylinders, the rows being perpendicular to the ΓX direction. Results for three different filling fractions f_s are shown: (a) 0.026, (b) 0.104, and (c) 0.415. Their analysis gives conclusions similar than that discussed above for the hexagonal cluster.

V. SUMMARY

In conclusion, it has been shown that SC slabs made of 2D distributions of rigid cylinders in air behaves for the

sound waves like Fabry-Perot cavities does for light waves. This work has presented a comprehensive study of this new class of acoustic interferometers recently introduced in Ref. 11. Their behavior as a function of the thickness and the lattice symmetry has been studied by a experimental technique which allows one to obtain the reflectance of finite structures. A theoretical description based on a self-consistent wave theory that contains all orders of multiple scattering has been proved to reproduce the experimental observations. On the other hand, a homogenization procedure has lead us to conclude that hexagonal lattice is isotropic with regards to sound propagation while the square lattice is biaxial. This phenomenon, which is similar to the one predicted in 2D photonic crystals based on hexagonal and square distributions of dielectric cylinders,[34] supports the paralelism between PC's and SC's. Also, the acoustic band structure has been obtained from the reflectance minima found in the spectra of finite systems. Finally, disordered structures that holds the lattice symmetry have been analyzed with our wave theory and we have conclude that perfect order is a basic condition to obtain the interference phenomena in a large region of frequencies below and above the band gaps.

ACKNOWLEDGMENTS

This work has been partially supported by the Comisión Asesora de Ciencia y Tecnología of Spain, Contract No. MAT00-1670-C04 and by the Centro de Estudios de America Latina (UAM-BSCH). We thank C. López and F. Meseguer for their comments, suggestions, and continuous support. We acknowledge the computing facilities provided by the Centro de Computación Científica at the Universidad Autónoma de Madrid. J.S.-D. also thanks valuable conversations with T. Ochiai.

*Author to whom the correspondence should be addresed. Electronic mail: jose.sanchezdehesa@uam.es

[1] J. Joannopoulos, R. Meade, and J. Winn, *Photonic Crystals, Molding the Flow of Light* (Princeton University Press, Princeton, NJ, 1995).
[2] J.P. Dowling, J. Acoust. Soc. Am. **91**, 2539 (1992).
[3] R. Martínez-Sala, J. Sancho, J.V. Sánchez-P érez, J. Llinares, and F. Meseguer, Nature (London) **378**, 241 (1995).
[4] J.V. Sánchez-Pérez, D. Caballero, R. Martí nez-Sala, C. Rubio, J. Sánchez-Dehesa, F. Meseguer, J. Llinares, and F. Gálvez, Phys. Rev. Lett. **80**, 5325 (1998).
[5] C. Rubio, D. Caballero, J.V. Sánchez-Pérez, R. Martínez-Sala, J. Sánchez-Dehesa, F. Meseguer, and F. Cervera, J. Lightwave Technol. **17**, 2202 (1999).
[6] D. Caballero *et al.*, Phys. Rev. E **60**, R6316 (1999).
[7] D. Caballero *et al.*, Phys. Rev. B **64**, 064303 (2001).
[8] W.M. Robertson and W.F. Rudy III, J. Acoust. Soc. Am. **69**, 3080 (1992).
[9] L. Sanchis, F. Cervera, J. Sánchez-Dehesa, J.V. Sánchez-Pérez, C. Rubio, and R. Mart ínez-Sala, J. Acoust. Soc. Am. **109**, 2598 (2001).
[10] M.S. Kuswaha, Appl. Phys. Lett. **70**, 3218 (1997).
[11] F. Cervera *et al.*, Phys. Rev. Lett. **88**, 023902 (2002).
[12] F.R. Montero de Espinosa, E. Jimenez, and M. Torres, Phys. Rev. Lett. **80**, 1208 (1998).
[13] J.O. Vasseur, P.A. Deymier, G. Frantziskonis, G. Hong, B. Djafari-Rouhani, and L. Dobrzynsky, J. Phys.: Condens. Matter **10**, 6051 (1998).
[14] M. Torres *et al.*, Phys. Rev. Lett. **82**, 3054 (1999).
[15] S. Yang, J.H. Page, Z. Liu, M.L. Cowan, C.T. Chan, and P. Sheng, Phys. Rev. Lett. **88**, 104301 (2002).
[16] M.M. Sigalas and E.N. Economou, J. Sound Vib. **158**, 377 (1992).
[17] M.S. Kuswaha, P. Halevi, L. Dobrzynski, and B. Djafari-Rhouhani, Phys. Rev. Lett. **71**, 2022 (1993).
[18] M.M. Sigalas and N. Economou, Europhys. Lett. **36**, 241 (1996).
[19] M.M. Sigalas and N. García, Appl. Phys. Lett. **76**, 2307 (2000).
[20] J.O. Vasseur *et al.*, Phys. Rev. Lett. **86**, 3012 (2001).
[21] Ph. Lambin *et al.*, Phys. Rev. E **63**, 066605 (2001).
[22] Z. Liu, C.T. Chan, P. Sheng, A.L. Goertzen, and J.H. Page, Phys. Rev. B **62**, 2446 (2000).
[23] Y.Y. Chen and Z. Ye, Phys. Rev. E **64**, 036616 (2001); Phys. Rev. Lett. **87**, 184301 (2001).
[24] V. Twersky, J. Acoust. Soc. Am. **24**, 42 (1951); J. Math. Phys. **3**, 700 (1962).
[25] R.D. Doolittle and H. Uberall, J. Acoust. Soc. Am. **39**, 272 (1966).
[26] S. Nojima, Appl. Phys. Lett. **79**, 1959 (2001).
[27] T. Ochiai and J. Sánchez-Dehesa, Phys. Rev. B **65**, 245111 (2002).
[28] For technical details see F.S. Ham and B. Segall, Phys. Rev. **124**, 1786 (1961).
[29] E. Meyer and E.G. Newman, *Physical and Applied Acoustics* (Academic Press, New York, 1972).
[30] N.D. Lang and W. Kohn, Phys. Rev. B **1**, 4555 (1970).
[31] D.H. Towne, *Wave Phenomena* (Dover, New York, 1988).
[32] K.W.-K. Shung and Y.C. Tsai, Phys. Rev. B **48**, 11 265 (1993).
[33] N. W. Ashcroft and N. D. Mermin, *Solid State Physics* (Harcourt College Publishing, Fort Worth, 1976), p. 101.
[34] P. Halevi, A.A. Krokhin, and J. Arriaga, Phys. Rev. Lett. **82**, 719 (1999); Appl. Phys. Lett. **75**, 2725 (1999).